Growing an Actin Gel on Spherical Surfaces

V. Noireaux,* R. M. Golsteyn,[†] E. Friederich,[†] J. Prost,* C. Antony,[†] D. Louvard,[†] and C. Sykes*

*Laboratoire Physico-Chimie "Curie," Unité Mixte de Recherche CNRS/Institut Curie (UMR 168), 75231 Paris Cedex 05, and [†]Laboratoire Compartimentation et Dynamique Cellulaire, Unité Mixte de Recherche CNRS/Institut Curie (UMR 144), 75248 Paris Cedex 05, France

ABSTRACT   Inspired by the motility of the bacteria *Listeria monocytogenes*, we have experimentally studied the growth of an actin gel around spherical beads grafted with ActA, a protein known to be the promoter of bacteria movement. On ActA-grafted beads F-actin is formed in a spherical manner, whereas on the bacteria a "comet-like" tail of F-actin is produced. We show experimentally that the stationary thickness of the gel depends on the radius of the beads. Moreover, the actin gel is not formed if the ActA surface density is too low. To interpret our results, we propose a theoretical model to explain how the mechanical stress (due to spherical geometry) limits the growth of the actin gel. Our model also takes into account treadmilling of actin. We deduce from our work that the force exerted by the actin gel on the bacteria is of the order of 10 pN. Finally, we estimate from our theoretical model possible conditions for developing actin comet tails.

INTRODUCTION

Actin polymerization plays a crucial role in cell motility. One of the most widely studied examples (Lackie, 1986; Stossel, 1993) is the crawling movement of eukaryotic cells by protrusion of actin-rich lamellipodia in front of the cell that tract the cell forward when the microfilament network reorganizes. The force induced by the growth of actin filaments is sufficient to stress and deform cell membranes. A similar system of force generation is also responsible for the movement of *Listeria monocytogenes* once in the cytoplasm of infected cells. By virtue of producing an F-actin filled-tail, *Listeria* constitute a simple model for studying movement induced by actin polymerization. The tail is made of microfilaments cross-linked together (Cossart, 1995) and oriented with their plus end (favored for polymerization) toward the bacterium. The protein responsible for F-actin nucleation has been identified (Kocks et al., 1992; Domann et al., 1992) as a transmembrane protein of 69 kDa called ActA. The mechanism of actin filament formation from *Listeria* has been studied in cell-free extracts of *Xenopus* eggs or human cell extracts, and shows that the recruitment of eukaryotic proteins is necessary for the motility of *Listeria* (Lasa and Cossart, 1996; Welch et al., 1997). Our goal was to experimentally study the role of topology on actin polymerization by conceiving a system that resembles that of *Listeria* but permits testing various parameters such as geometry or density of actin nucleators. We prepared and purified a recombinant ActA and grafted it covalently onto beads of different diameters. When added to cell-free extracts prepared from HeLa cells, the beads acquired an F-actin gel structure. The thickness of this actin gel around the beads was found to be dependent in a reproducible manner upon the diameter of the bead. Indeed, the gel is built by addition of G-actin at the surface of the bead, which necessarily creates a stress in a spherical geometry. This stress is sufficient to limit the growth of the actin gel. In a first approximation (i.e., if we neglect treadmilling), one can state that the polymerization process stops when the chemical energy gain in the polymerization (E_χ) is balanced by the elastic energy cost for adding a new monomer (E_{el}). If we designate ξ the average distance between nucleating proteins (nucleators) on the bead (the density of nucleators is then $1/\xi^2$), $\Delta\mu$ the chemical energy released in the polymerization process, r_i the radius of the bead, then $E_\chi = 1/\xi^2 \Delta\mu \times 4\pi r_i^2$. The work of the force for adding a monomer is $\sigma_{rr}a$ per unit area, where σ_{rr} is the radial component of the stress and a is the size of a G-actin monomer, then the elastic energy can be expressed as $E_{el} = \sigma_{rr}a \times 4\pi r_i^2$. From the expression of σ_{rr} derived in this paper (Eq. 17), we deduce $E_{el} \cong C(e/r_i)^2 a \times 4\pi r_i^2$, where C is the elasticity modulus of the actin gel and e is its thickness. Writing $E_{el} = E_\chi$ gives $e = r_i \sqrt{\Delta\mu/Ca\xi^2}$, which expresses that e is an increasing function of the bead size, as experimentally observed. This simple model applies for equilibrium situations. In the experimental system we analyze here, the polymerization process is stationary but not at equilibrium, and the model presented takes into account the simultaneous polymerization/depolymerization process (or treadmilling) as well as the stress created by the actin gel on the spherical bead.

MATERIALS AND METHODS

Construction, expression, and purification of the GST-ActA-His variant

DNA manipulations were performed by routine procedures (Sambrook et al., 1989). In a first step, the sequence 5′-GGATCCGGTCTAGAG-AAGCTTCCCGAATTC-3′ (encoding *Xba*I and *Hind*III within *Bam*HI and *Eco*RI) was inserted in the pGEX2T expression vector (Amersham Pharmacia Biotech, Uppsala, Sweden) yielding pGEX2T-adaptor. In a

second step, an oligonucleotide 5′-CTAGACCCGGGCCCATCACCAT-CACCATCACTG-3′ (encoding six histidines and comprising *Sma*I and *Eco*RI sites at the 5′ and 3′ ends, respectively) was inserted in the pGEX2T-adaptor yielding pGEX2T-his. The third step consisted of introducing a DNA fragment encoding the ActA protein truncated of its transmembrane anchor and the signal peptide. The pCB6-actA1 (Friederich et al., 1995) expression vector was linearized by *Eco*RI and filled in using the Klenow fragment of DNA polymerase I. After heat-inactivation of the enzyme, the DNA was digested with *Xba*I and an ∼1.75-kb *Xba*I-*Eco*RI blunt-ended actA gene fragment was isolated. Finally, the actA fragment was ligated into *Xba*I-*Sma*I-digested pGEXT2T-his. The final pGEX2T-actA-his construct encodes GST fused to ActA comprising a six-histidine tag in the C-terminal region (see Fig. 1 *A*). GST-ActA-His was produced in *Escherichia coli* strain BL21 (DE3) and purified successively on a nickel agarose matrix (purchased from Qiagen GmbH, Hilden, Germany) and on a Sepharose glutathione matrix (purchased from Amersham Pharmacia Biotech, Uppsala, Sweden). The elution solution was dialyzed in buffer D (0.2 M boric acid, pH 8.5) and stored in aliquots at −80°C. Protein concentration was determined as described by Bradford (1976), (reagents purchased from Bio-Rad, Hercules, CA).

Fluorescent actin preparation

Rabbit skeletal muscle actin was prepared according to the method described by Spudich and Watt (1971). Actin was labeled with rhodamine using the procedure of Kreis et al. (1982). Aliquots were stored at −80°C at a concentration of 2 mg/ml (40 μM). Phalloidin was purchased from Sigma-Aldrich (St. Quentin Fallavier, France) and directly added to the samples to a final concentration of 0.3 μg/ml.

Latex beads

Latex beads were purchased from Polyscience, Inc. (Warrington, PA): we used carboxylate functionalized latex beads for covalent grafting (25 μEq/g of carboxylate groups). Diameters of particles were chosen in the 1-to-10 μm range. Proteins were covalently grafted via EDAC (1-ethyl-3-(-3-dimethylaminopropyl)carbodiimide)) as described by the manufacturer. ActA-grafted beads were stored at 4°C in a storage buffer (20 mM phosphate buffer, pH 7.4, 1% BSA, 150 mM NaCl, 20 mM NaN$_2$, 0.5% glycerol). We made two series of ActA-grafted beads. The first series (we will call this series "ActA saturated beads") with beads of various diameters (1 μm, 2 μm, 10 μm) was prepared by incubating the beads in excess of ActA to saturate the protein surface concentration. The amount of protein coupled to the beads was determined by subtracting the quantity of protein remaining in the supernatant after incubation from the initial amount of protein in the solution. The total surface of the beads was deduced from their volume and size. The surface concentration of grafted proteins was then given by the ratio between the total amount of coupled proteins versus the total surface of the beads. As an example, the concentration of ActA on 10-μm-diameter beads was estimated at $(5.6 \pm 0.6) \times 10^{-2}$ protein/nm^2 (we reproducibly measured that ∼14 ± 3 μg protein could be bound to 100 μl of a suspension of 2.5% of 10-μm-diameter latex beads), assuming a molecular mass of GST-ActA-His of 92,890 Da. The second series of beads (we will call this series "ActA concentration beads") was prepared to vary the surface density of ActA protein. The beads were incubated in a mixture of ActA and BSA at a ratio of 10, 30, 50, 70, and 90% of ActA. The total amount of coupled proteins was determined by the same method as the previous series, and the amount of ActA proteins coupled to the beads was deduced, according to the manufacturer instructions, by SDS-PAGE analysis of proteins remaining in solution (see Table 1). We found that the surface density of ActA did not correspond to the relative amount of BSA/ActA in the solution, due to the different affinity of BSA and ActA to carboxylated functions.

Listeria bacteria

We used a modified *L. monocytogenes* strain described by Lasa et al. (1995). This strain carries a deletion removing the actA gene and was transformed with a multicopy plasmid encoding ActA.

Cell line

The human HeLa S3 cell line was grown in Dulbecco's minimum essential medium (DMEM) supplemented with 10% fetal calf serum, at 37°C, under 5% CO$_2$.

HeLa cell-free extracts

Cytosolic extracts were prepared following a modification of the procedure described by Paschal and Gerace (1995). About 10^9 cells were centrifuged at $300 \times g$ for 10 min and washed twice in PBS, resuspended in 5 ml buffer A (5 mM HEPES, pH = 7.4, 5 mM potassium acetate, 2 mM magnesium acetate, 1 mM EGTA, and a cocktail of protease inhibitors including Pefablock, leupeptin, pepstatin, and aprotinin at 1 μM each), and stirred slowly at 4°C for 20 min on a rotary shaker. The solution was passed five times in a cell cracker and centrifuged for 30 min at $40,000 \times g$, 4°C. The supernatant was clarified by centrifugation for 60 min at $100,000 \times g$. Finally, aliquots of cytosolic extracts (12 mg/ml) were frozen in liquid nitrogen and stored at −80°C.

Gel electrophoresis and immunoblotting

Proteins were analyzed by SDS-PAGE. Immunoblotting was made by use of the antibody anti-ActA2 against the N-terminus of ActA (Golsteyn et al., 1997). Transfer to nitrocellulose and antibody incubation were performed according to the method described by Burnette (1981).

Methods of observation

Beads were directly taken from the storage buffer. *Listeria* were first suspended in half the volume of Xb buffer (10 mM Hepes, pH = 7.7, 100 mM KCl, 1 mM MgCl$_2$, 0.1 mM CaCl$_2$, 50 mM sucrose) before adding to cell-free extracts supplemented with 30 mM creatine phosphate, and 1 mM ATP as described by Marchand et al. (1995). In each case the volume increase did not exceed 15% of the initial volume of the extracts.

Fluorescence microscopy

Observations were made of beads or bacteria in extracts containing a final concentration of 0.5 μM rhodamine actin. A 1-μl suspension of 2.5% beads in storage buffer (or from the resuspended *Listeria* in Xb buffer) was resuspended in 10 μl of cell-free extracts supplemented with rhodamine actin, creatine phosphate, and ATP. Five μl of the mixture was squashed between a microscope slide and a 22-mm-square coverslip sealed with varnish. Samples were observed by fluorescence microscopy with an inverted microscope (IX70, Olympus Optical Co. Gmbh, Hamburg, Germany).

Electron microscopy

Samples for observation were prepared as described by Tilney and Portnoy, 1989. A number *n* μl of 2.5% bead solution in storage buffer (or 8 μl resuspended *Listeria* in 10 times less volume of Xb) was added to 100 μl of cell-free extracts supplemented with ATP and creatine phosphate. *n* was calculated to have the same total bead surface for the different samples:

$n = 4$ or 8, respectively, for 1- and 2-μm-diameter beads; for 10-μm-diameter beads, we took 8 μl from 5× reconcentrated beads in storage buffer. The mixture was incubated 4 h at room temperature. The latex beads and/or the bacteria were pelleted in a horizontal centrifuge (3000 RPM for 3 min), and incubated for 40 min at 4°C with 1% glutaraldehyde, 0.5% of tannic acid in phosphate buffer, 50 mM, pH = 6.3, rinsed twice in phosphate buffer, incubated 20 min at 4°C in phosphate buffer containing 0.5% osmium, rinsed three times with water, and stained with an aqueous solution of 2% uranyl acetate for 1 h at 4°C. The samples were then dehydrated in alcohol and embedded in epon. Gold labeling was performed by incubating 4 μl beads in a solution (2.5% BSA in PBS) containing 1/150 of the polyclonal rabbit antibody anti-ActA2 against the N-terminus of ActA (Golsteyn et al., 1997). Then, after washing, the beads were incubated with protein A coupled to 10 nm gold particles (PAG10) purchased from Dr. J. W. Slot, Department of Cell Biology, Utrecht University, The Netherlands. Ultrathin sections (thickness 70 ± 10 nm) stained with ethanolic uranyl acetate and lead citrate were observed in a Philips CM 120 electron microscope at 80 kV.

RESULTS

Purification of GST-ActA-His

The protein ActA was first purified on a nickel agarose matrix and further on a Sepharose glutathione matrix. The purity of the protein was confirmed by SDS-PAGE under reducing conditions. Coomassie staining of the gel (Fig. 1 *B*) revealed one protein band migrating at a position corresponding to an apparent molecular mass of 120 kDa that was higher than expected from the amino acid sequence (see Fig. 1 *A*): 92 kDa. It is likely that this apparent migration behavior is due to the high proline content of ActA (Kocks et al., 1992). Antibodies against ActA reacted with this band, confirming that indeed this band corresponded to ActA.
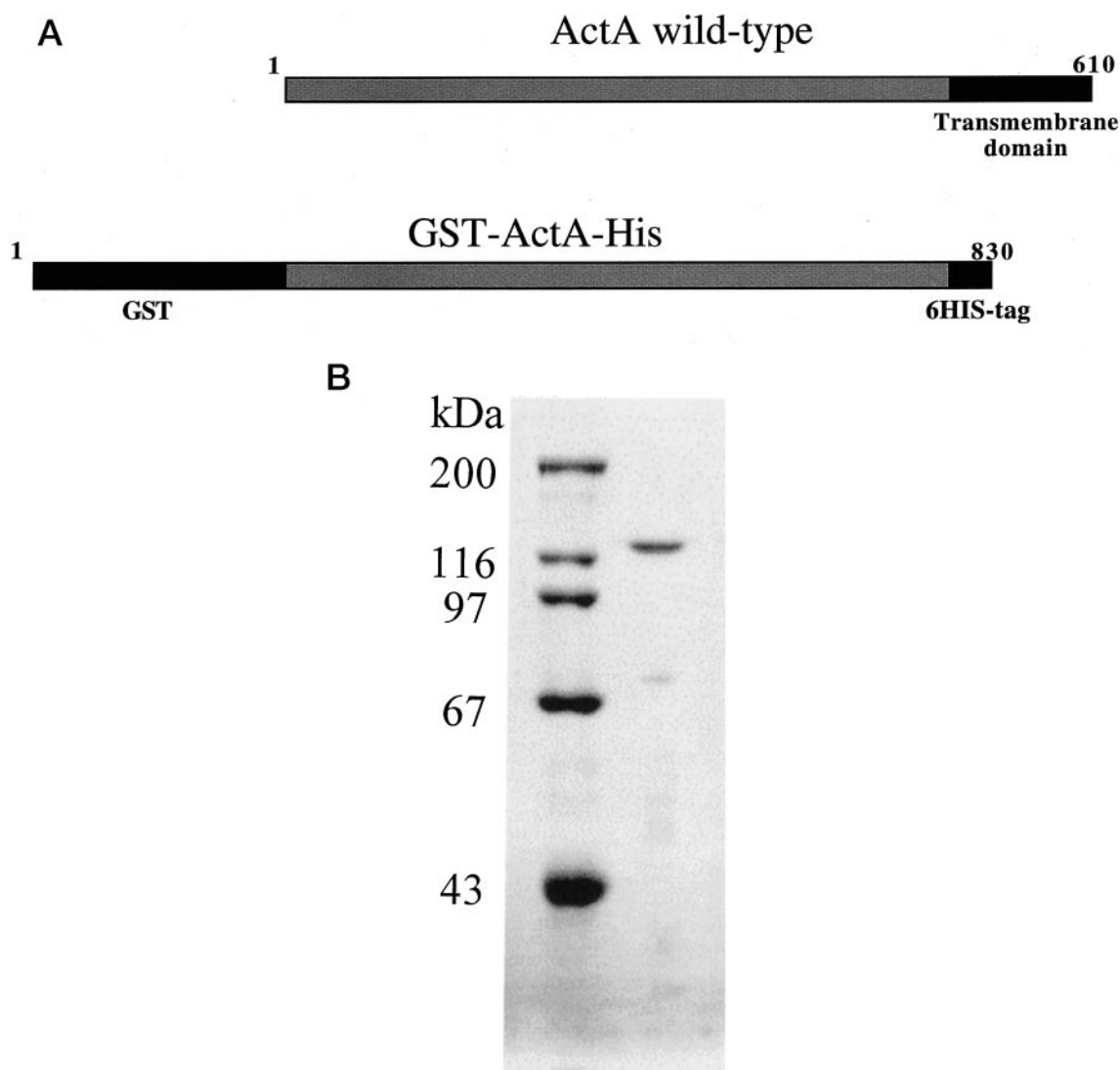

FIGURE 1 (*A*) Diagram describing GST-ActA-His, the variant of ActA used for our experiments. Amino acid numbers are shown. (*B*) SDS-PAGE analysis of the purified protein GST-ActA-His (*right column*) and molecular weight marker proteins marker (*left column*).

Experimental assay: *Listeria* in cell-free extracts prepared from HeLa cells

We set up an assay for studying *Listeria* in vitro in cell-free extracts prepared from HeLa cells. Cell-free extracts were supplemented with ATP, creatine phosphate, and rhodamine actin as described in Materials and Methods. During the incubation ~40% of *Listeria* developed an F-actin tail, and the length of the comet-like tail ranged from 15 to 30 μm. The velocity of *Listeria* varied between 0.75 ± 0.5 μm/min within a population of 30 moving *Listeria*. Some of the comets displayed a periodic density (see Fig. 2). A similar phenomenon has been described for an ActA truncated variant of *Listeria* (Lasa et al., 1997). Immobile *Listeria* were surrounded with an isotropic F-actin cloud and did not form any comet-like tail.

ActA saturated beads in cell-free extracts prepared from HeLa cells

GST-ActA-His was covalently grafted to polystyrene beads functionalized with COOH (of 1 μm, 2 μm, and 10 μm in diameter). These beads were added to cell-free extracts supplemented with rhodamine actin as described in the experimental assay for *Listeria*. We confirmed that the

FIGURE 2 Mixture of beads 2 μm in diameter (*round objects*) coated with GST-ActA-His and *Listeria monocytogenes* (*elongated objects*) a few hours after incubation in HeLa cell-free extracts. Fluorescence microscopy.

quantity of ActA detached from the beads was negligible ($<5\%$) by analyzing the extracts after incubation with the 2-μm-diameter beads by immunoblotting with ActA specific antibodies. Within 30 min the beads were surrounded by a fluorescent staining (see beads of 2-μm-diameter on Fig. 2), whose intensity increased with time, indicating the accumulation of actin around the beads. The beads were easily detected by phalloidin staining (0.3 μg/ml final concentration), which revealed that this actin structure was composed of F-actin. Growth of the actin gel was stabilized after 4 h, as confirmed by video time-lapse microscopy observations. At this time the beads reduced their Brownian motion and became stuck to the bottom slide.

To test whether the quantity of F-actin accumulated around beads and around bacteria was the same, we mixed beads and *Listeria* in one preparation (Fig. 2): the fluorescence intensity was indeed equivalent for beads and bacteria (within a relative error of 10%). After 4–5 h the actin gel around the beads stopped growing, whereas *Listeria* continued to develop an F-actin tail.

The three following tests confirm the specificity of ActA for F-actin gel growth:

- The same type of carboxylate latex beads (2 μm in diameter) grafted with BSA did not recruit rhodamine actin (the quantity of grafted BSA was estimated at 2×10^{-1} molec./nm^2) under the same conditions;
- uncoupled carboxylated beads did not nucleate an actin gel as well;
- we tested that actin nucleation was not a simple effect due to the presence of lysine in ActA (although the global charge of ActA is expected to be negative in physiological conditions, since the calculated isoelectric point of GST-ActA-His is 5), as polylysine, under certain experimental conditions, is reported to nucleate actin polymerization (filaments are oriented with their pointed end toward the nucleating surface) (Brown and Spudich, 1979): we repeated the experimental assay in cell-free extracts with beads coated with polylysine instead of ActA. We used three types of polylysine (ref. P8920, P0899, P1149 purchased from Sigma). In none of the three samples, under similar experimental conditions, did we observe any fluorescence due to actin assembly (long filaments, ~50 μm, appearing after 24 h are of a very different nature). We checked that our polylysine was indeed functional: beads grafted with polylysine placed in a buffer containing 0.5 M KCl, 0.5 mM MgCl$_2$, 0.2 mg/ml G-actin did nucleate F-actin, as described by Brown and Spudich (1979). Under these conditions, beads grafted with ActA did not generate actin filaments when placed in buffer containing 0.5 M KCl, 0.5 mM MgCl$_2$, 0.5 mM rhodamine actin, supplemented with G-actin to a final concentration of 0.2 mg/ml actin. This is consistent with the report that incubation of *Listeria*

with actin alone did not result in actin association with bacteria (Welch et al., 1997).

We cut the GST part of GST-ActA-His with thrombin: we obtained four segments including the GST segment, but three others as well despite the fact that no other site of ActA was supposed to react with thrombin. We did the same experiments on the ActA-grafted latex beads with GST-ActA-His, and got the GST segment only. Fluorescence microscopy observations of these latter beads in the extracts (actin marked with rhodamine) showed the same behavior as nontreated beads: this shows that the presence of GST does not affect, in a significant way, the polymerization process.

We examined the protein-grafted beads and the *Listeria*, incubated in cell-free extracts for 4 h, by electron microscopy to observe their surrounding actin gel in detail. Two important observations were made (see Fig. 3). First, neither the 2-μm-diameter beads grafted with BSA nor the uncoupled carboxylated beads produced an actin gel: this confirms the observations made by fluorescence microscopy. Second, the thickness of the actin gel produced by GST-ActA-His-grafted beads was found to vary with the radius of the beads. Third, we examined actin structures and confirmed that both the beads coated with ActA and *Listeria* produced similar F-actin gels.

The effect of ActA concentration on beads in cell-free extracts

The role of ActA density was studied by preparing beads that contained different ratios of BSA and ActA. These beads were incubated in supplemented cell-free extracts and observed both by fluorescence microscopy and electron microscopy. The estimated densities of ActA are given in Table 1. We confirmed that the density of ActA around one bead was homogeneous by gold labeling (see Fig. 4) for the beads with the highest and the lowest density. The amount of PAG10 around one bead was found to be 63.3 ± 30 PAG/bead on the $3.8 \pm 0.6 \times 10^{16}$ prot./m^2 beads by counting 13 beads on ultrathin sections that crossed the bead through its center. Fluorescence microscopy revealed that the fluorescence intensity decreased when the ActA density decreased.

The thickness e of the actin gel layer around both ActA saturated beads and ActA concentration beads is given in Table 1; e was measured on images taken at the same magnification ($\times 28,000$). We examined ~ 100 beads and performed a statistical analysis on a random population of 15 beads, making 20 measurements per bead. If the ultrathin section did not cross the bead right through its center, a gray ring of width d (projection of the bead edge) was visible around the latex beads on the images. The radial thickness

e of the actin gel was deduced from:

$$e \cong \frac{\varepsilon}{\sqrt{1 + \left(\dfrac{d}{\delta}\right)^2}}$$

where ε is the F-actin thickness measured on the image, and $\delta = 70 \pm 10$ nm the thickness of the section (see Materials and Methods). The correcting factor $1/[\sqrt{1 + (d/\delta)^2}]$ does not qualitatively change the experimental results, but reduces the dispersion. The variation of the bead size for the 1- and 2-μm beads was within 4% (see Table 1). Although the size range of the 10-μm calibrated beads was within 10%, it happened that we observed beads as large as 20 μm, and we took advantage of this variation to make measurements of actin gel size around one of these larger beads. We estimated its radius R from the electron microscopy image by using geometrical arguments, which give:

$$R \cong r \sqrt{1 + \left(\dfrac{d}{\delta}\right)^2}$$

where r is the radius of the bead section on the image, and d is defined above.

The experimental values in Table 1 show that 1) the consequence of a decrease in ActA surface density is that no actin gel is formed, below a density of the order of 3×10^{16} prot./m^2; and 2) the thickness of the actin gel around ActA saturated beads is an increasing function of the radius of the bead.

DISCUSSION

Let us now try to understand quantitatively why, in a spherical geometry, the polymerization stops when a given thickness of actin gel is reached. In this context, the word "gel" means that actin filaments are cross-linked in a network that resists both static and shear compression. Any addition of G-actin material at the particle/gel interface requires the buildup of a stress able to push away the already formed gel. Within the time scales over which the polymerization process takes place the gel is clearly in mechanical equilibrium. The following model simultaneously takes into account that actin is polymerizing at the surface of the sphere (i), depolymerizing at the outer end (e), and that the gel is constrained. Our notations are summarized in Fig. 5.

Let dn^{i}/dt and dn^{e}/dt be, respectively, the number of monomers added to the gel per unit time at the surface of the bead (i) and at the outer surface of the gel (e); according to van't Hoff (1884) one can write:

$$\frac{dn^{i}}{dt} = \omega_1^{b} \cdot c^{i} - \omega_2^{b} \tag{1a}$$

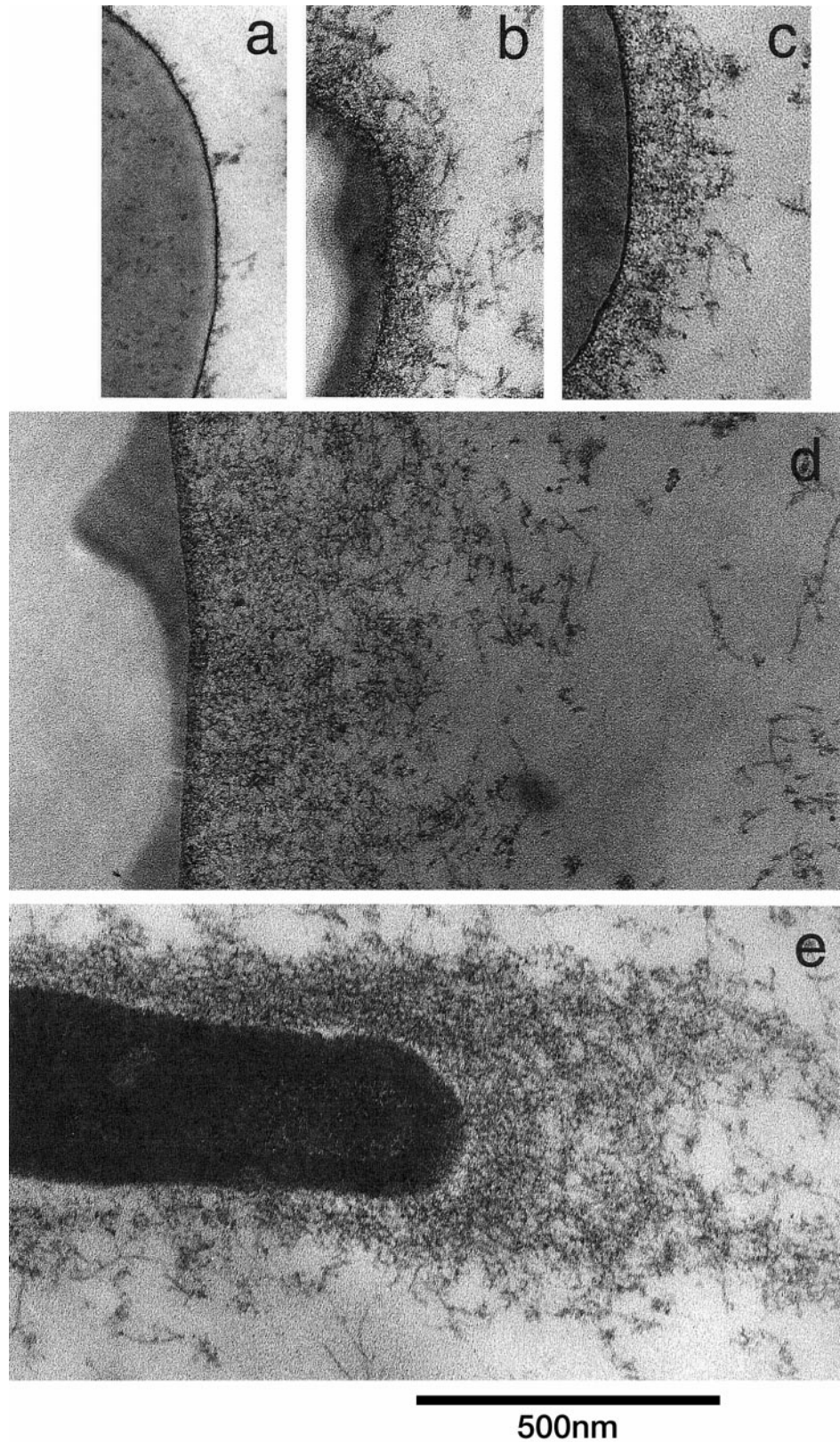$$\frac{dn^{e}}{dt} = \omega_1^{p} \cdot c^{e} - \omega_2^{p} \tag{1b}$$

FIGURE 3 Electron micrographs of latex beads (or *Listeria*) incubated in HeLa cell-free extracts. (*a*) Latex beads ($\phi = 2\ \mu$m) coated with BSA; (*b*) latex beads ($\phi = 1\ \mu$m) coated with GST-ActA-His; (*c*) latex beads ($\phi = 2\ \mu$m) coated with GST-ActA-His; (*d*) latex beads ($\phi = 10\ \mu$m) coated with GST-ActA-His; (*e*) bacterium with its actin comet tail. One can observe that the beads are slightly deformed, probably because of processing for EM analysis.

where c^i and c^e are, respectively, the concentration of free G-actin monomers at the surface of the bead and at the outer surface. ω_1^b and ω_1^p are the polymerization rates for barbed (*b*) ends and pointed (*p*) ends, and ω_2^b and ω_2^p are the probability for a monomer to leave the filament at the barbed (*b*) and pointed (*p*) end. This notation (*b* and *p*)
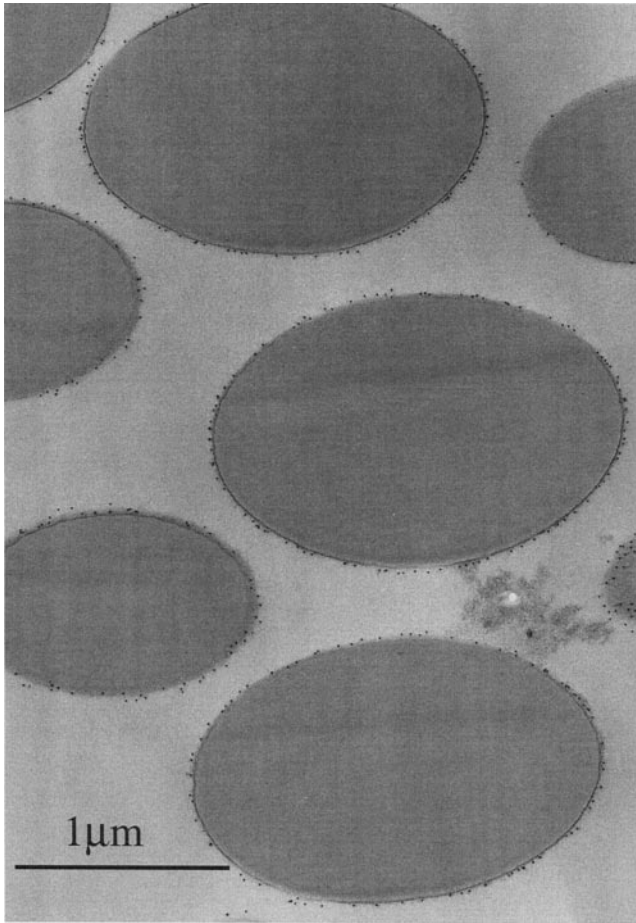
FIGURE 4 Immuno-gold (10 nm) labeling of beads grafted with $3.8 \pm 0.6 \times 10^{16}$ ActA/m^2. Beads are deformed due to EM processing.

implies that the actin filaments are oriented with their barbed end toward the beads surface, and their pointed end toward the outer part of the gel. This assumption is in agreement with electron microscopy observations on *Listeria* comets (Tilney et al., 1992) but we have no direct experimental evidence of actin filament polarity on beads. However, as an indirect proof, the model based on this assumption accounts for experimental results.

Considering that polymerization of actin filaments occurs on the surface of the bead, the inner part of the gel is stressed, which means that the coefficients ω_1^b and ω_2^b of dn^i/dt depend on the stress $\sigma = \sigma_{rr}(r_i)$. First we calculate the stress created by the actin gel on a bead. Second, we theoretically describe the general situation that includes diffusion of G-actin monomers and treadmilling of actin filaments. We discuss the different possible regimes and show that in our experimental conditions, treadmilling is essentially negligible. We show that, in this limit, the thickness of the grown gel depends on the radius of the bead, as measured experimentally. We end up in discussing the possible conditions under which beads can nucleate a comet tail made of actin filaments.

Expression of the stress $\sigma(r, t)$ as a function of r_i and the Young's modulus of the gel

The radial component of the stress $\sigma_{rr}(r, t)$ and the tangential component $\sigma_{\perp\perp}(r, t)$ of the stress $\sigma(r, t)$, must obey the equilibrium equation (in spherical coordinates).

$$\vec{\nabla} \cdot \underline{\underline{\sigma}}(r, t) = 0 = \frac{1}{r^2} \frac{\partial}{\partial r} r^2 \sigma_{rr}(r, t) + \frac{2}{r} \sigma_{\perp\perp}(r, t) = 0 \qquad (2)$$

A spherical layer of area $4\Pi r_i^2$ and volume $4\Pi r_i^2 dr_i$, initially polymerized (synthesized) and cross-linked at the particle surface at time t', is converted after a time $(t - t')$ to a spherical layer of area $4\Pi r(t)^2$ and volume $4\Pi r(t)^2 dr(t)$. The tangential component of the stress can be simply evaluated as (Landau and Lifchitz, 1967):

$$\sigma_{\perp\perp}(r, t) = C\left(\frac{r(t) - r_i}{r_i}\right) \qquad (3)$$

where C is the elasticity modulus of the gel.

The validity of Eq. 3 requires that the gel deformation is small enough, that it can be considered in the linear elasticity regime. Considering that the observed thicknesses are of the order of a few hundred nanometers for several micron diameter spheres, this is a reasonable approximation.

Let us define the outer radius of the gel by $r_e(t)$. At time $t = 0$, $r_e(t = 0) = r_i$. Furthermore, at any given time, the absence of external stress on the gel surface is expressed by:

$$\sigma_{rr}(r_e, t) = 0 \qquad (4)$$

Making use of Eqs. 2–4, one can calculate the radial component of the stress as a function of radius vector r:

$$\sigma_{rr}(r, t) = 2C\left[\frac{r_e^2(t)}{r^2}\left(\frac{r_e(t)}{3r_i} - \frac{1}{2}\right) - \frac{r}{3r_i} + \frac{1}{2}\right] \qquad (5)$$

As a result, the gel exerts a stress $\sigma_{rr}(r = r_i, t) = \sigma(t)$ on the bead surface, given by:

$$\sigma(t) = 2C\left[\frac{r_e^2(t)}{r_i^2}\left(\frac{r_e}{3r_i} - \frac{1}{2}\right) + \frac{1}{6}\right] \qquad (6)$$

This stress in turn controls the polymerization rate at the bead surface.

Steady-state treadmilling regime

In the stationary regime, the gel thickness $e = r_e - r_i$ is independent of time; polymerization at the inner surface exactly balances depolymerization at the outer surface and a monomer diffusive flux transports the monomers from the outer surface to the inner one. This implies:

$$\frac{dn^i}{dt} = -\frac{dn^e}{dt} \qquad (9)$$

$$r^2 J_C(r) = \text{const,} \qquad (10)$$

TABLE 1 Thickness of the actin gel as a function of the radius of the beads

r_i (μm)	Estimate of the ActA Density	e (nm)	Quotient e/r_i
0.48 ± 0.02	saturated ($5.6 \pm 0.6 \, 10^{16}$ prot./m^2)	94 ± 10	2×10^{-1}
0.95 ± 0.04	saturated ($5.6 \pm 0.6 \, 10^{16}$ prot./m^2)	146 ± 10	1.5×10^{-1}
4.72 ± 0.48	saturated ($5.6 \pm 0.6 \, 10^{16}$ prot./m^2)	503 ± 20	1×10^{-1}
10.1 ± 0.5	saturated ($5.6 \pm 0.6 \, 10^{16}$ prot./m^2)	790 ± 20	0.8×10^{-1}
0.95 ± 0.04	$3.8 \pm 0.6 \, 10^{16}$ prot./m^2	125 ± 10	1.3×10^{-1}
0.95 ± 0.04	$2.3 \pm 0.4 \, 10^{16}$ prot./m^2	small aggregates of actin ($\leq$40 nm)	
0.95 ± 0.04	$2.1 \pm 0.3 \, 10^{16}$ prot./m^2	small aggregates of actin ($\leq$40 nm)	
0.95 ± 0.04	$1.7 \pm 0.3 \, 10^{16}$ prot./m^2	no actin detected	
0.95 ± 0.04	$6.2 \pm 1 \, 10^{15}$ prot./m^2	no actin detected	

r_i is the average radius of the beads given by the manufacturer, except in the line where $r_i = 10.1 \, \mu$m is out of range (twice the average size, see the Discussion); e is the thickness of the actin gel around beads of various diameters; the estimate of the density of grafted ActA is measured as described in Materials and Methods.

and

$$r^2 J_C(r) = r_i^2 J_C(r_i) = (r_i + e)^2 J_C(r_e) = r_i^2\left(-\frac{dn^i}{dt}\right)\xi^{-2} \quad (11)$$

in which $J_C(r)$ is the flux (algebraic value) of monomeric actin (G-actin), and ξ the average distance between ActA molecules.

As usual, the diffusion flux can be expressed in terms of the gradient of the monomeric concentration $C(r)$, and the monomer diffusion coefficient D:

$$J_C(r) = -D\frac{dC(r)}{dr} \quad (12)$$

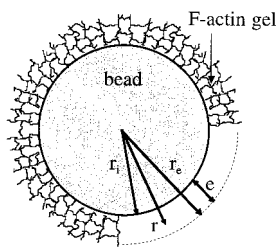If we can take D as a constant, then Eqs. 10 and 12 give:

$$J_C(r) = -D\frac{c^e - c^i}{e} \cdot \frac{r_i(r_i + e)}{r^2} \quad (13)$$

where c^e and c^i stand for the concentration of monomers outside the gel and at the bead surface, respectively.

Combining Eqs. 9, 11, and 13, we obtain:

$$\frac{dn^i}{dt}(\sigma, c^i) = -\frac{dn^e}{dt} = D\frac{c^e - c^i}{e}\left(1 + \frac{e}{r_i}\right)\xi^2. \quad (14)$$

That is, with Eqs. 1 and after elimination of c^i:

FIGURE 5 Notations used in the text. r_i is the radius of the bead, r and θ the spherical coordinates, e is the thickness of the gel layer. $r_e = r_i + e$.

$$\omega_1^b(\sigma)\left(c^e + (\omega_1^p c^e - \omega_2^p)\frac{e}{D\xi^2\left[1 + \dfrac{e}{r_i}\right]}\right) - \omega_2^b(\sigma) = \omega_2^p - \omega_1^p c^e \quad (15)$$

Equation 15 determines the gel thickness e as a function of the polymerization rates, their stress dependence, the diffusion coefficient D, the ActA density ξ^{-2}, the external monomeric concentration c^e, and the particle radius r_i. This is a treadmilling regime in which the polymerization rate is governed by the stress buildup and monomer diffusion, rather than by an adjustment of the monomer concentration, as would be the case in solution (Carlier et al., 1997).

Gel thickness at steady state

The rates $\omega_1^b(\sigma)$ and $\omega_2^b(\sigma)$ can be related to the stress-free rates $\omega_1^b(0)$ and $\omega_2^b(0)$ by a simple use of Kramers or Eyring rate theories (Eyring, 1935; Kramers, 1940) in which the potential barriers to be overcome for either adding or subtracting a monomer are shifted by the mechanical work against addition or for subtraction of the monomer at the barrier maximum. As usual, k is the Boltzmann constant and T the temperature (S.I. unit).

Hence:

$$\omega_1^b(\sigma) = \exp(-\xi^2 a_1 \sigma/kT)\omega_1^b(0) \quad (16a)$$

$$\omega_2^b(\sigma) = \exp(+\xi^2 a_2 \sigma/kT)\omega_2^b(0). \quad (16b)$$

The force acting on a single filament is $\sigma\xi^2$, and a_1, a_2 are the distances over which the force produces work to reach the maximum of the potential barrier. In a simple picture, $a_1 + a_2 \cong a$, where a is the size of a G-actin monomer. Equation 6 expressing the stress σ can be simplified when $e \ll r_i$:

$$\sigma \cong C\left(\frac{e}{r_i}\right)^2 \quad (17)$$

If we further remark that under most practical circumstances $\omega_1^p c^e \ll \omega_2^p$, we can rewrite Eq. 15 in the form:

$$c^e \omega_1^b(e/r_i) \times \left(1 - \frac{e/e^*}{(1 + (e/r_i))}\right) = \omega_2^b(e/r_i) + \omega_2^p \qquad (18)$$

where two important lengths clearly emerge: the bead radius r_i and the diffusion length $e^* = D\xi^2 c^e/\omega_2^p$. They correspond to two different possibilities of reaching steady state: either the stress buildup is so large that the polymerization rate essentially drops to zero, or the diffusion becomes so slow that the monomer concentration at the bead surface becomes small enough that it is balanced by the depolymerization at the outer surface.

Diffusion-limited regime

Let us first consider $r_i \gg e^*$ (i.e., essentially flat surfaces, no stress can build up); knowing from Eq. 18 that $e < e^*$, Eq. 18 simplifies to:

$$c^e \omega_1^b(0) \times \left(1 - \frac{e}{e^*}\right) = \omega_2^b(0) + \omega_2^p \qquad (19)$$

or

$$e = e^* \left(1 - \frac{(\omega_2^p + \omega_2^b(0))}{c^e \omega_1^b(0)}\right) \qquad (20)$$

If we further remark that under usual circumstances the stress-free initial polymerization rate $c^e \omega_1^b(0)$ is much larger than both the depolymerization rate at the pointed end ω_2^p and the stress-free depolymerization rate at the barbed end $\omega_2^b(0)$, then

$$e \approx e^* \qquad (21)$$

Note that at steady state in this regime, the polymerization rate is $c^i \omega_1^b(0) - \omega_2^b = \omega_2^p$ ($c_i \ll c_e$). The concentration at the bead surface reaches the steady-state treadmilling concentration obtained in solution (Carlier et al., 1997).

Stress-limiting regime

Let us now consider the opposite limit $e^* \gg r_i$; anticipating that $r_i \geq e$, Eq. 18 reads:

$$c^e \omega_1^b\left(\frac{e}{r_i}\right) = \omega_2^p + \omega_2^b\left(\frac{e}{r_i}\right). \qquad (22)$$

Clearly, in this regime the gel thickness is governed by the bead radius thickness. Whenever ATP hydrolysis is not directly involved in the polymerization process [note that ATP hydrolysis occurs later, once the polymerization has taken place and detailed balance should hold], one can write:

$$\frac{\omega_1^b(0)}{\omega_2^b(0)} = v \times \exp(\Delta\mu_1/kT) \qquad (23a)$$

$$c^e \frac{\omega_1^b(0)}{\omega_2^b(0)} = \exp(\Delta\mu/kT) \qquad (23b)$$

where v is the reaction volume, $\Delta\mu_1$ the chemical potential difference per monomer, between the unpolymerized state and the polymerized state excluding the translational entropy $kT \times \ln(c^e v)$, and $\Delta\mu$ the chemical potential difference per monomer including the translational entropy. $\Delta\mu$ represents the chemical energy released in the polymerization process. Using Eq. 16 and Eq. 23b we get:

$$\frac{c^e \omega_1^b(\sigma)}{\omega_2^b(\sigma)} = \exp\left(\frac{\Delta\mu - \sigma\xi^2 a}{kT}\right) \qquad (24)$$

Dividing Eq. 22 by ω_2^b, one can extract:

$$\sigma\xi^2 a = \Delta\mu - kT \times \ln\left(1 + \frac{\omega_2^p}{\omega_2^b(\sigma)}\right) \qquad (25)$$

In principle, Eq. 25 is only an implicit equation for σ, and hence for e/r_i. However, the ratio ω_2^p/ω_2^b comes only in a logarithm, and it only appears as a corrective term. If we ignore the logarithm, Eq. 25 expresses the fact that the polymerization stops in this regime, when the mechanical work required to add a new monomer equals the chemical energy gained in the process. The depolymerization at the pointed end appears as a correction to this basic feature (unless the depolymerization rate under stress is unexpectedly small).

Transforming Eq. 25 into an equation for the gel thickness by using Eq. 17, we get:

$$e = e^{**} = r_i\left(\frac{\Delta\tilde{\mu}}{C\xi^2 a}\right)^{1/2} \qquad (26)$$

in which we have written $\Delta\tilde{\mu} = \Delta\mu - kT \times \ln(1 + \omega_2^p/\omega_2^b)$.

The gel thickness is proportional to the bead radius, which simply expresses that there is one stress value for which steady state is reached.

General case and orders of magnitude

Equation 18 may be easily solved, for instance graphically as shown in Fig. 6. The general solution gives values intermediate between e^* and e^{**}. More important are the estimates of e^* and e^{**}. In our experiments, in which the distance between ActA molecules on the surface is 42–77 Å (see Materials and Methods; Table 1), we take a mesh size which is the smallest possible length imposed by the actin filament diameter: $\xi = 10$ nm; the concentration in free G-actin in the HeLa cell extracts is expected to be of the order of 0.5 μM, as suggested by the critical concentrations
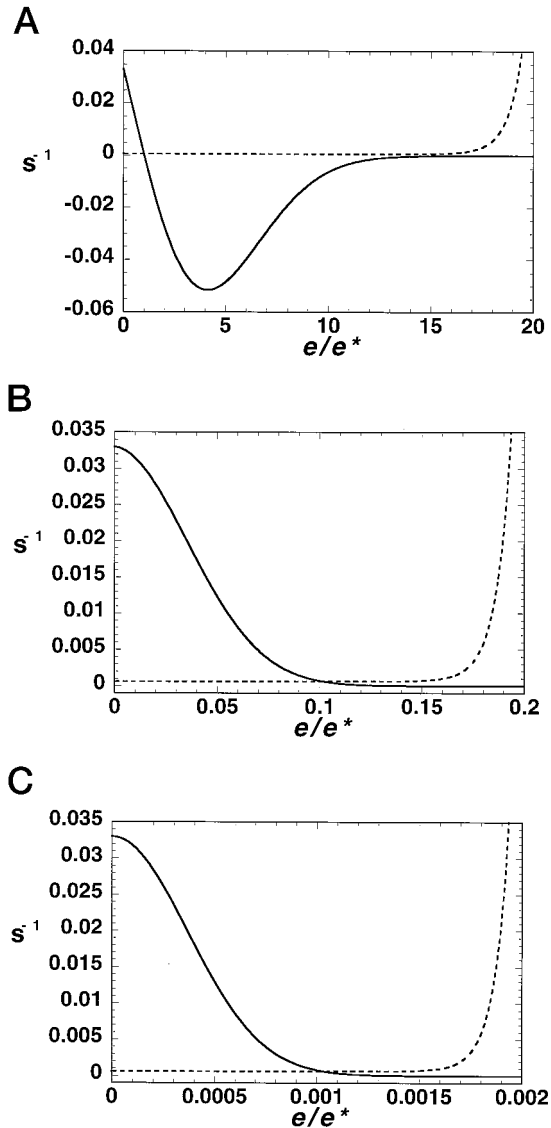
FIGURE 6 Graphic solutions for Eq. 18 are obtained by rewriting Eq. 18 using Eqs. 16a and b, taking for the sake of argument $a_1 = a_2 = a/2$, which leads to:

$$c^e \omega_1^b(0) \times \exp\left(-\alpha\left(\frac{e^*}{r_i} \times \frac{e}{e^*}\right)\right)\left[1 - \frac{e/e^*}{1 + e/r_i}\right]$$

$$= \omega_2^b(0) \times \exp\left(+\alpha\left(\frac{e^*}{r_i} \times \frac{e}{e^*}\right)\right) + \omega_2^p,$$

with

$$\alpha = \frac{\xi^2 aC}{2kT};$$

the left and right part of the above equation are, respectively, represented bold and dashed; the numerical values needed are the ones given in the text:

$$\omega_2^p \cong 6 \times 10^{-4} \text{s}^{-1}, \xi \cong 100 \text{ Å}, a \cong 50 \text{ Å}, l_p \cong 15 \text{ } \mu m,$$

$$C \approx \frac{kT l_p}{\xi^4}, c^e \omega_1^b(0) \cong 3.3 \times 10^{-2} \text{s}^{-1}$$

of actin filaments dynamics (Carlier, 1991), since we are in a situation where the pointed ends depolymerize. This gives a c^e value of 3×10^{14} molec./cm^3; ω_2^p can be estimated (Theriot et al., 1992) from our observations on *Listeria* as the ratio between the velocity of the bacteria (0.75 μm/min) and the length of the comet (20 μm): we get $\omega_2^p \approx 6 \times 10^{-4}$ s^{-1}. The value of the monomeric diffusion coefficient of G-actin has been measured in a buffer (buffer A: 2 mM Tris (pH = 8), 0.2 mM CaCl$_2$, 1.0 mM ATP, 0.5 mM dithiothreitol [DTT]): $D_b = 5 \times 10^{-7}$ cm^2/s (Lanni et al., 1981). Knowing that the viscosity of cell-free extracts is about three times that of water (or buffer) (Fushimi and Verkman, 1991), we infer a value $D \approx 1.6 \times 10^{-7}$ cm^2/s in our experiments. Hence we expect e^* to be of the order of 1 mm. This estimate represents an upper limit, since steric hindrance and temporary interactions of monomers with the gel proteins could slow down the diffusion process. In any case this length is large compared to the experimentally found thicknesses, and one expects the experiment to correspond to the stress-governed regime.

The radius dependence of the gel thickness observed experimentally (Table 1) confirms these expectations. Equation 26 gives us a prescription for estimating the proportionality ratio expected between e and r_i. If we take the gel elastic modulus $C \cong (K/\xi_c^4) = (kT l_p/\xi_c^4)$ in which $K = kT l_p$ is the bending elastic modulus of actin filaments, l_p their persistence length, and ξ_c the average distance between cross-links, we get:

$$\frac{e}{r_i} \cong \left(\frac{\Delta\mu}{kT}\right)^{1/2} \frac{\xi_c^2}{\xi(l_p a)^{1/2}}. \quad (27)$$

With $\Delta\mu \sim 14 \ kT$ (Gordon et al., 1976), $\xi_c \cong \xi \cong 10^{-6}$ cm, $l_p \cong 15 \ \mu$m (Yanagida et al., 1984; Ott et al., 1993; Gittes et al., 1993; Drögemeier and Eimer, 1994; Isambert et al., 1995), $a_p \approx 5 \times 10^{-7}$ cm, we obtain $(e/r_i) \cong 10^{-1}$, which is typically what we observe experimentally. We can thus conclude that the polymerization process in our experiment is indeed stopped by the mechanical stress buildup. Note that the above-discussed numbers imply an elastic modulus C (a few 10^6 Pa, given that $\xi \approx 10^{-6}$ cm) large compared to values measured with actin gels. If we take as an upper limit of C the largest value measured in the *Listeria* comet (F. Gerbal et al., submitted for publication), i.e., $C \approx 10^4$ Pa, we are led with a length $\xi \approx 3 \times 10^{-6}$ cm, which implies that not all ActA are functional at the surface. We

as estimated from the slope S of the experimental curve giving the thickness e versus time: $S = 200$ (nm)/20 $\times$ 60 (s) (V. Noireaux, manuscript in preparation) by writing $c^e \omega_1^b(0) = S/a$, then $\omega_2^b(0) = 2.7 \times 10^{-8}$ s^{-1} as deduced from Eq. 24. (*a*) Taking $e^*/r_i = 10^{-2}$, $e = e^*$ is the solution, as described in the text; (*b*) taking $e^*/r_i = 1$ gives the solution $e/e^* = 10^{-1}$; (*c*) taking $e^*/r_i = 10^2$, the solution is $e/e^* = 0.001$, and consequently $e \cong e^{**}$ and $e/r_i = 10^{-1}$ as measured experimentally.

then find $(e/r_i) \approx 0.3$, which is still compatible with our experiments.

Spherical symmetry versus "comet"

The above-developed arguments show that if the polymerization process takes place on a spherically symmetric substrate, the growth stops automatically at a given thickness. This will always be the case unless a symmetry-breaking transition takes place. A very rough estimate of this symmetry-breaking possibility goes as follows: at the outer surface, although the normal stress vanishes, the tangential stress (given by Eq. 3) is at its maximum: the gel is under tangential tension. In general, beyond a given threshold, solid materials under tension break. The threshold value depends on material properties, but most of the time it can be expressed as a deformation threshold (i.e., a strain threshold), which turns out to be of order one. In other words, when $(r_e - r_i)/r_i = (e/r_i) \approx 1$, the gel is very likely to develop a fracture. This fracture releases a significant amount of the tensile stress at the interior of the gel layer, and consequently also a sizable amount of the normal stress at the inner surface. The polymerization process can then go on, and one can understand that a comet can result from this initial fracture. For this to occur, one wants (from Eq. 27):

$$\left(\frac{\Delta\mu}{kT}\right)^{1/2} \frac{\xi_c^2}{\xi(l_p a)^{1/2}} \approx 1. \qquad (28)$$

Since $\Delta\mu$ is essentially of order 10 kT, and l_p, a are not subject to large changes, one needs a ratio (ξ_c^2/ξ) as large as possible to have chances of observing symmetry breaking according to this mechanism. It is striking to remark that native *Listeria* develop comets containing $\sim 10^3$ filaments per cross section of the comet, which corresponds to an average distance between ActA of ~ 100 nm: if we assume $\xi_c \approx \xi$, condition 28 is then essentially fulfilled. Note, however, that in our experiments ξ_c and ξ are clearly different, since varying ξ moderately can result in the absence of the gel.

In this argument, the size of the particle does not play a role. This is correct as long as we ignore fluctuations. The relevant fluctuations are ActA surface density fluctuations that are frozen during the grafting process. As a rough rule of thumb they are of the order of $\sqrt{N}$, where N is the total number of ActA on the bead. Typically one-half of the bead will have an ActA excess of $\sqrt{N}$ over the other half: this considerably decreases the instability threshold. The exact conditions under which a comet could develop go beyond the scope of this work. We can easily understand that the smallest bead radius compatible with a gel formation will be the best, since this corresponds to the largest relative unbalance. This is confirmed by recent observations made by the group of J. A. Theriot (Cameron et al., 1999), who propose an alternative mechanism involving the stochastic-

ity of the polymerization process of actin filaments (van Oudenaarden and Theriot, 1999).

CONCLUSIONS

This work confirms the crucial role played by ActA in actin polymerization and demonstrates the interest of studying this process in a spherical topology. If there were no cross-linking of the actin filaments one would observe the growth of a polymerized layer bound only by the diffusion length e^* (see Discussion). Our results show unambiguously that the factor limiting the thickness of the actin gel is the mechanical stress exerted by the gel on the bead surface. The fact that an external force could modify the polymerization process of microtubules or actin filaments has been previously analyzed theoretically (Hill and Kirschner, 1982). In our work, the force per filament necessary to block polymerization is found to be of the order of 10 pN, which is quite reasonable (i.e., 10 kT per monomer size). It does not provide either strong support or strong opposition to any molecular theory (Mogilner and Oster, 1996). It is interesting to realize that the pressure exerted by the gel on the bead is of the order of one atmosphere. Scaling this pressure with ActA density allows us to estimate the maximum force a native *Listeria* is able to develop: we find a force of the order of a few nanonewtons, much larger than adverse forces a cell could oppose [note, however, that buckling of the *Listeria* comet would drastically decrease this force (Gerbal et al., 1999)]. Our observations are very close to the one made by M. Dogterom on microtubules polymerization (Dogterom and Yurke, 1997): the orders of magnitude are fairly similar. In this last experiment, measurements are made on single microtubules and the force is due to the existence of an external obstacle. In our case the force results from the self-developed stress bound to the spherical topology. Note that a native *Listeria* has globally the same topology, so that our work demonstrates the importance of mechanical stresses in *Listeria* as well. Finally, it is interesting to remark that the incidence of spherical topology on polymeric growth properties has been pointed out in other contexts; for instance, the problem of "starburst polymers" (de Gennes and Hervet, 1983), where the coordination number of the reacting entity should change at a certain radius because of steric hindrance. In this case, the polymerization that takes place at the outer edge of the star is not stopped, but the number of bonds allowed in the reaction decreases.

REFERENCES

Bradford, M. M. 1976. A rapid and sensitive method for the quantitation of microgram quantities of protein utilizing the principle of protein-dye binding. *Anal. Biochem.* 72:248–254.

Brown, S. S., and J. A. Spudich. 1979. Nucleation of polar actin filament assembly by a positively charged surface. *J. Cell Biol.* 80:499–504.

Burnette, W. N. 1981. Western blotting: electrophoretic transfer of proteins from sodium dodecyl sulfate-polyacrylamide gels to unmodified nitro-cellulose and radiographic detection with antibody and radioiodinated protein A. *Anal. Biochem.* 112:195–203.

Cameron, L. A., M. J. Footer, A. van Oudenaarden, and J. A. Theriot. 1999. Motility of ActA protein-coated microspheres driven by actin polymerization. *PNAS.* 96:4908–4913.

Carlier, M.-F. 1991. Actin:protein structure and filament dynamics. *J. Biol. Chem.* 266:1–4.

Carlier, M.-F., V. Laurent, J. Santolini, R. Melki, D. Didry, G.-X. Xia, Y. Hong, N.-H. Chua, and D. Pantaloni. 1997. Actin depolymerizing factor (ADF/Cofilin) enhances the rate of filament turnover: implication in actin-based motility. *J. Cell Biol.* 136:1307–1323.

Cossart, P. 1995. Actin based bacterial motility. *Curr. Opin. Cell Biol.* 7:94–101.

de Gennes, P. G., and H. Hervet. 1983. Statistics of "starburst" polymers. *Phys. Lett.* 44:351–360.

Dogterom, M., and B. Yurke. 1997. Measurement of the force-velocity relation for growing microtubules. *Science.* 278:856–860.

Domann, E., J. Wehland, M. Rohde, S. Pistor, M. Hartl, W. Goebel, M. Leimeister-Wächter, M. Wuenscher, and T. Chakraborty. 1992. A novel bacteria virulence gene in *Listeria monocytogenes* required for host cell microfilament interaction with homology to the proline-rich region of vinculin. *EMBO J.* 11:1981–1990.

Drögemeier, J., and W. Eimer. 1994. Polarized and depolarized dynamic light scattering study of F-actin in solution: comparison with model calculations. *Macromolecules.* 27:96–101.

Eyring, H. 1935. The activated complex in chemical reactions. *J. Chem. Phys.* 3:107–115.

Friederich, E., E. Gouin, R. Hellio, C. Kocks, P. Cossart, and D. Louvard. 1995. Targeting of *Listeria monocytogenes* ActA protein to the plasma membrane as a tool to dissect both actin-based cell morphogenesis and ActA function. *EMBO J.* 14:2731–2744.

Fushimi, K., and A. S. Verkman. 1991. Low viscosity in the aqueous domain of cell cytoplasm measured by picosecond polarization microfluorimetry. *J. Cell Biol.* 112:719–725.

Gerbal, F., V. Noireaux, C. Sykes, F. Jülicher, P. Chaikin, A. Ott, J. Prost, R. M. Golsteyn, E. Friederich, D. Louvard, V. Laurent, and M.-F. Carlier. 1999. On the "Listeria" propulsion mechanism. *PRAMANA–Journal of Physics.* 53:1–16.

Gittes, F., B. Mickey, J. Nettleton, and J. Howard. 1993. Flexural rigidity of microtubules and actin filaments measured from thermal fluctuations in shape. *J. Cell Biol.* 120:923–934.

Golsteyn, R. M., M. C. Beckerle, T. Koay, and E. Friederich. 1997. Structural and functional similarities between the human cytoskeletal protein zyxin and the ActA protein of *Listeria monocytogenes. J. Cell Sci.* 110:1893–1906.

Gordon, D., Y.-Z. Yang, and E. Korn. 1976. Polymerization of *Acanthamoeba* actin. *J. Biol. Chem.* 251:7474–7479.

Hill, T. L., and M. W. Kirschner. 1982. Bioenergetics and kinetics of microtubule and actin filament assembly-disassembly. *Int. Rev. Cytol.* 78:1–125.

Isambert, H., P. Venier, A. C. Maggs, A. Fattoum, R. Kassab, D. Pantaloni, and M.-F. Carlier. 1995. Flexibility of actin filaments derived from thermal fluctuations. *J. Biol. Chem.* 270:11437–11444.

Kocks, C., E. Gouin, M. Tabouret, P. Berche, and P. Cossart. 1992. *Listeria monocytogenes*-induced actin assembly requires the actA gene product, a surface protein. *Cell.* 68:521–531.

Kramers, H. A. 1940. Brownian motion in a field of force and the diffusion model of chemical reactions. *Physica (Utrecht).* 7:284–304.

Kreis, T. E., B. Geiger, and J. Schlessinger. 1982. Motility of microinjected rhodamine actin within living chicken gizzard cells determined by fluorescence photobleaching recovery. *Cell.* 29:835–845.

Lackie, J. M. 1986. Cell movement and cell behaviour. Allen and Unwin, London.

Landau, L., and E. Lifchitz. 1967. Theory of Elasticity. Mir, URSS.

Lanni, F., D. L. Taylor, and B. R. Ware. 1981. Fluorescence photobleaching recovery in solutions of labeled actin. *Biophys. J.* 35:351–364.

Lasa, I., and P. Cossart. 1996. Actin-based motility: towards a definition of the minimal requirements. *Trends Cell Biol.* 6:109–114.

Lasa, I., V. David, E. Gouin, J.-B. Marchand, and P. Cossart. 1995. The amino-terminal part of ActA is critical for the actin-based motility of *Listeria monocytogenes*; the central proline-rich region acts as a stimulator. *Mol. Microbiol.* 18:425–436.

Lasa, I., E. Gouin, M. Goethals, K. Vancompernolle, V. David, J. Vandekerckove, and P. Cossart. 1997. Identification of two regions in the N-terminal domain of ActA involved in the actin comet tail formation by *Listeria monocytogenes. EMBO J.* 16:1531–1540.

Marchand, J.-B., P. Moreau, A. Paoletti, P. Cossart, M.-F. Carlier, and D. Pantaloni. 1995. Actin-based movement of *Listeria monocytogenes*: actin assembly results from the local maintenance of uncapped filament barbed ends at the bacterium surface. *J. Cell Biol.* 130:331–343.

Mogilner, A., and G. Oster. 1996. Cell motility driven by actin polymerization. *Biophys. J.* 71:3030–3045.

Ott, A., M. Magnasco, A. Simon, and A. Libchaber. 1993. Measurement of the persistence length of polymerized actin using fluorescence microscopy. *Phys. Rev. E.* 48:1642–1645.

Paschal, B. M., and L. Gerace. 1995. Identification of NTF2, a cytosolic factor for nuclear import that interacts with nuclear pore complex protein p62. *J. Cell Biol.* 129:925–937.

Sambrook, J., E. F. Fritsch, and T. Maniatis. 1989. Molecular Cloning. A Laboratory Manual, 2nd ed. Cold Spring Harbor Laboratory Press, Cold Spring Harbor, NY.

Spudich, J. A., and S. Watt. 1971. The regulation of rabbit skeletal muscle contraction. I. Biochemical studies of the interaction of the tropomyosin-troponin complex with actin and the proteolytic fragments of myosin. *J. Biol. Chem.* 246:4866–4871.

Stossel, T. P. 1993. On the crawling of animal cells. *Science.* 260:1086–1094.

Theriot, J. A., T. J. Mitchinson, L. G. Tilney, and D. A. Portnoy. 1992. The rate of actin-based motility of intracellular *Listeria monocytogenes* equals the rate of actin polymerization. *Nature.* 357:257–260.

Tilney, L. G., D. J. DeRosier, A. Weber, and M. S. Tilney. 1992. How *Listeria* exploits host cell actin to form its own cytoskeleton. II. Nucleation, actin filament polarity, filament assembly, and evidence for a pointed end capper. *J. Cell Biol.* 118:83–93.

Tilney, L. G., and D. A. Portnoy. 1989. Actin filaments and the growth, movement, and spread of the intracellular bacterial parasite, *Listeria monocytogenes. J. Cell Biol.* 109:1597–1608.

van Oudenaarden, A., and J. A. Theriot. 1999. Cooperative symmetry-breaking by actin polymerization in a model for cell motility. *Nat. Cell Biol.* 1:493–499.

van't Hoff, J. H. 1884. Etudes de Dynamique Chimique. F. Muller, Amsterdam.

Welch, M. D., A. DePace, S. Verma, A. Iwamatsu, and T. J. Mitchison. 1997. The human Arp2/3 complex is composed of evolutionarily conserved subunits and is localized to cellular regions of dynamic actin filament assembly. *J. Cell Biol.* 138:375–384.

Welch, M. D., A. Iwamatsu, and T. J. Mitchison. 1997. Actin polymerization is induced by Arp2/3 protein complex at the surface of *Listeria monocytogenes. Nature.* 385:265–269.

Yanagida, T., M. Nakase, K. Nishiyama, and F. Oosawa. 1984. Direct observation of motion of single F-actin filaments in the presence of myosin. *Nature.* 307:58–60.